Editors' Suggestion

Signature of magnon polarons in electron relaxation on terbium revealed by comparison with gadolinium

Bo Liu [1,*] Huijuan Xiao [1] Gesa Siemann [1] Jonathan Weber [1] Beatrice Andres,[1] Wibke Bronsch [1] Peter M. Oppeneer [2] and Martin Weinelt [1,†]

[1]*Freie Universität Berlin, Fachbereich Physik, Arnimallee 14, 14195 Berlin, Germany*

[2]*Department of Physics and Astronomy, Uppsala University, P. O. Box 516, 75120 Uppsala, Sweden*

(Received 7 May 2021; revised 2 July 2021; accepted 6 July 2021; published 28 July 2021)

Magnons and phonons are elementary excitations of spin and lattice systems that can form a hybrid quasiparticle in the presence of strong magnetoelastic coupling. Here we use spin-, angle-, and energy-resolved photoemission spectroscopy to show that magnon-phonon hybridization plays an important role for the relaxation of the electron surface-state in Tb, opening both majority and minority spin channels in electron-phonon scattering. This is attributed to the strong $4f$ spin-orbit coupling, as evidenced by a comparison of the lifetime broadening in the occupied surface states of Gd and Tb. Both ferromagnetic metals have a comparable valence electronic structure, but the magnetocrystalline anisotropy is much stronger in Tb as compared to Gd. Consequently, in Gd electron-phonon and electron-magnon scatterings lead to spin-dependent photohole relaxation rates. Unlike in Gd, the lifetime broadening of the occupied surface state in Tb is only weakly spin dependent and the mass enhancement parameter λ is twice the spin-averaged value of Gd. This difference in phase space is explained by the intimate coupling of phonons and magnons to form magnon polarons, which opens both minority and majority spin bands as decay channels.

DOI: 10.1103/PhysRevB.104.024434

I. INTRODUCTION

When magnons and phonons are strongly interacting due to large magnetoelastic coupling in magnetic materials, hybridized modes, i.e., the coupled propagation of spin and elastic waves emerge at the crossing points of otherwise undisturbed magnon and phonon branches [1]. Such magnon polarons have been shown to facilitate spin control in oxides such as yttrium iron garnet [2] and can further lead to an enhancement of spin pumping and spin Seebeck effect in regions where phonon and magnon dispersions hybridize [3,4]. In contrast to this in ferromagnetic metals the magnetization dynamics are usually determined by the valence electronic system. Conduction electrons allow for spin transport via superdiffusive currents [5] and electron-phonon scattering leads to local spin flips and effective transfer of angular momentum to the lattice [6]. As these processes are intrinsically ultrafast they dominate spin dynamics on the femtosecond timescale. Generally it is argued that direct spin-lattice coupling leads to slower picosecond dynamics [7–9]. It allows us, for example, to control the magnetization by acoustic pulses modifying the magnetocrystalline anisotropy without heating the sample [10,11].

An obvious question is, what happens to electronic excitations in ferromagnetic metals when phonons and magnons are strongly coupled? To study the effect of spin-lattice coupling on spin-dependent electron dynamics, rare-earth metals are excellent model systems as their magnetic properties strongly depend on $4f$ electron occupancy while lattice vibrational modes vary weakly [12,13]. In particular, rare-earth metals have large magnetoelastic coefficients due to the large $4f$ orbital momentum of the ions, with the exception of Gd where the $4f$ orbital is exactly half filled and the orbital momentum disappears ($L = 0$) [12]. Very early studies by inelastic neutron scattering have shown strong spin-lattice coupling, for example in Tb, directly evidenced by avoided crossings of magnon and phonon dispersion branches [12]. Eschenlohr *et al.* reported a two-step demagnetization in $Gd_{1-x}Tb_x$ alloys where the second step varies with the Tb concentration. This change in the demagnetization has been attributed to the strong $4f$ spin-lattice coupling of the Tb atoms [9]. Our recent study suggests that already the fs-demagnetization in Tb is launched by $4f$ spin-lattice coupling via ultrafast magnon generation thereby showing a clear difference to Gd [14]. Nevertheless, direct evidence of the effect of $4f$ spin-lattice coupling on the magnetic moments of the $5d$ valence states near the Fermi surface remains elusive. This is of great importance to fully understand ultrafast magnetization dynamics as spins from different bands, e.g., from surface and bulk states seem to behave quite differently [15,16].

In this work we use spin-, angle-, and energy-resolved photoemission spectroscopy (PES) to study the role of magnon-phonon coupling in photohole relaxation by comparing the occupied component of the $5d_{z^2}$ surface state of Gd and Tb. At finite temperature the surface state shows spin mixing, which allows us to study the linewidth Γ of both its minority and majority spin components. We observe that below the bulk Debye temperature $\Theta_D \sim 160$ K, the spin

*boliu@zedat.fu-berlin.de
†weinelt@physik.fu-berlin.de

minority component of the Gd surface state exhibits a larger linewidth than its majority counterpart $\Gamma_{min} > \Gamma_{maj}$ [17,18]. Albeit less pronounced, this difference is also observed for Tb and attributed to electron-magnon scattering. With increasing temperature ($T \geqslant \Theta_D$), spin-mixing increases and electron-phonon scattering becomes dominant. Gd shows a spin-dependent mass-enhancement parameter λ with the increase in linewidth ($d\Gamma/dT \propto \lambda$) which is larger for the spin-majority channel ($\lambda_{maj} > \lambda_{min}$). In contrast to this no spin dependency of λ has been observed for the Tb surface state. Furthermore, our experimentally determined value of lambda is twice as large as the spin-averaged value of Gd. This suggests that in Tb electron-phonon scattering goes hand in hand with magnon emission and absorption, i.e., the formation of magnon polarons opens both spin channels for photohole relaxation.

II. EXPERIMENTAL METHODS

In the PES measurements we ionize the weakly bound surface states of Gd and Tb by laser pulses with a photon energy of 4.62 eV. The ultraviolet pulses are obtained via third harmonic generation of the 1.55 eV fundamental of a Ti:sapphire laser oscillator. The photo-emitted electrons are collected by a cylindric sector analyzer (CSA 300, Focus) and guided to the spin detector, which uses back reflection at an oxygen-passivated Fe/W(001) target [19]. Exchange scattering at the Fe film in combination with the 80 MHz repetition rate of the laser setup are essential to achieve sufficient statistics to determine the spin dependence of the surface state linewidth.

Hexagonal close-packed Gd and Tb thin films with (0001) orientation were prepared on a W(110) substrate by molecular beam epitaxy at room temperature. The tungsten substrate was cleaned following the standard recipe [20]. Surface order was confirmed by low electron energy diffraction (LEED). The deposition rate was monitored by a quartz microbalance to obtain a film thickness of 10 nm. To obtain higher crystallinity, Gd and Tb films were annealed at 780 K and 880 K for 3 and 1 minute, respectively. The pressure during film growth and PES measurements was 2×10^{-10} and 2×10^{-11} mbar, respectively. The Gd and Tb magnetic thin films were remanently magnetized in-plane by sending a current pulse through an airwounded coil inserted below the sample. This leads to homogeneously magnetized films as also seen from our magnetic linear dichroism measurements in Refs. [14,21]. The spin polarization is measured by reverting the magnetization of the Fe film on the W(001) scattering crystal. All data has been evaluated assuming a Sherman function of $S = 0.23$. Further details of the experiment may be found in Ref. [22]. We used liquid nitrogen to cool the sample and controlled its temperature by radiation heating using a double-helical filament to avoid magnetic stray fields. All spectra are taken at the Brillouin zone (BZ) center $\overline{\Gamma}$ under normal emission with an angular resolution of $\pm 2.5^\circ$.

III. RESULTS

Figure 1 shows the spin-resolved PE spectra of the surface state on (a) Gd and (b) Tb for different sample temperatures.

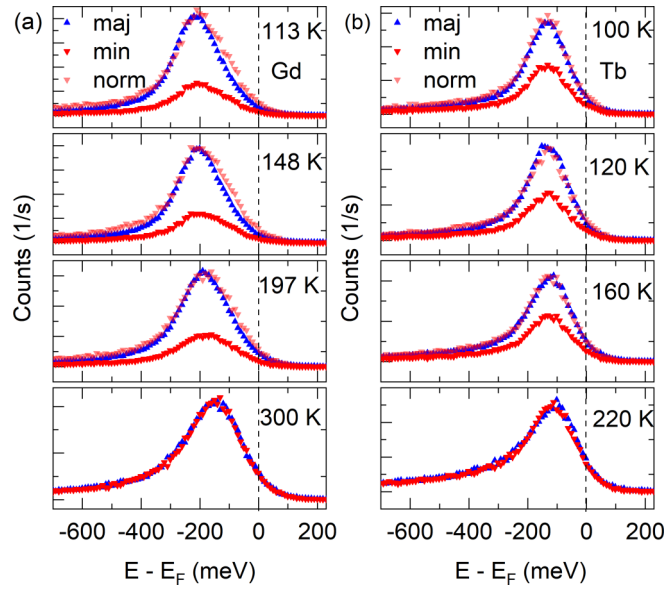

FIG. 1. Spin-resolved photoemission spectra of the d_{z^2} surface state on (a) Gd and (b) Tb as a function of the binding energy recorded at selected temperatures. Blue (up) and red (down) triangles represent spin majority and spin minority components of the occupied surface state, respectively. With increasing temperature the surface state shows stronger spin mixing. Dashed lines mark the Fermi energy. The photon energy was 4.62 eV.

The blue (up-pointing) and red (down-pointing) triangles represent the intensity of the spin majority and spin minority components, respectively. The lighter red symbols further represent as well the spin minority component of the surface state but normalized to its spin majority counterpart by multiplication. Gd and Tb are prototype systems for spin mixing [23,24], which manifests *inter alia* in a finite spin polarization of the occupied surface state component at finite temperature. With increasing temperature, the spin polarization drops and vanishes at the Curie temperature T_C of 293 K and 220 K for Gd and Tb, respectively. At the same time the exchange splitting remains finite even above T_C leading to well separated occupied and unoccupied components of the surface state [23]. This spin mixing or band mirroring behavior is summarized in Fig. 2. The binding energy $E_B = E_F - E$ of the occupied surface state in Fig. 2(a) stays clearly below the Fermi energy E_F, while the spin polarization in Fig. 2(b) vanishes at the Curie temperature T_C (indicated by dashed vertical lines).

As evident from Fig. 1(a) for the Gd surface state below T_C the linewidth of the spin minority channel is larger than the linewidth of its spin majority counterpart ($\Gamma_{min} > \Gamma_{maj}$). This difference reaches a maximum at low temperatures. At the same time it is obvious from Fig. 1(b) that the spin majority and the normalized spin minority components (lighter red symbols) of the Tb surface state nearly coincide, showing already in the raw data a similar linewidth for both spin channels ($\Gamma_{min} \simeq \Gamma_{maj}$).

Due to the low photon energy we probe a small parallel momentum range of only ± 0.03 Å^{-1}. Based on the small negative dispersion of the surface-state bands on Gd

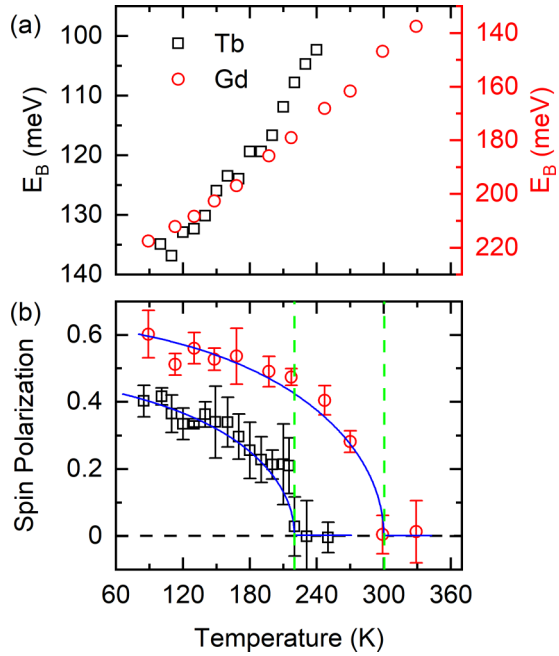

FIG. 2. (a) Binding energy and (b) spin polarization of the occupied d_{z^2} surface state on Gd and Tb as a function of temperature. The blue solid lines in (b) are fits using the Brillouin function B_J with $J = 7/2$ for Gd and $J = 6$ for Tb.

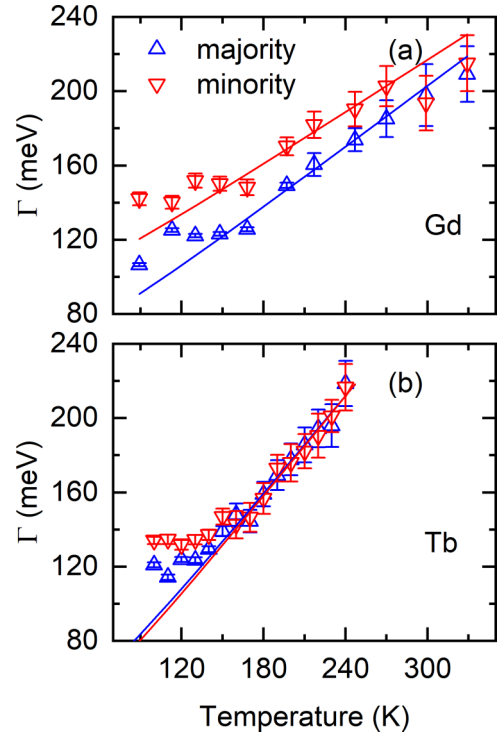

FIG. 3. Extracted linewidths Γ of the surface state on (a) Gd and (b) Tb for both the spin-majority (blue, up-triangle) and spin-minority (red, down-triangle) components as a function of temperature. The lighter red symbols represent as well the spin minority component of the surface state but normalized to its spin majority counterpart by multiplication. For temperatures above $T \geqslant 180$ K, the linewidth of the Gd surface state scales linearly with temperature (solid lines). For $T \leqslant 180$ K the linewidth Γ is obviously larger for the spin-minority than for the spin-majority channel, indicating the impact of spin-dependent electron-magnon scattering (magnon emission and absorption). In contrast, the linewidth of the Tb surface state shows very weak spin dependence, which we attribute to the formation of magnon polarons.

($m^* = -1.21\ m_e$) [18] and Tb [25] we fitted the spin-resolved data by a single Lorentzian function representing the surface state superimposed on a proper linear background and cut by the Fermi distribution as detailed in the Supplemental Material (SM) [26]. The fitting function is convolved with a Gaussian function with a full width at half maximum of 100 meV. The Gaussian represents the total energy resolution of our experiment set by the cylindrical sector analyzer (determined by the width of the low energy cutoff and the measured bandwidth of the ultraviolet (UV) laser pulse, see SM). The fitted Lorentzian linewidth Γ as a function of temperature for Tb and Gd thin films is shown in Figs. 3(a) and 3(b), respectively.

The linewidth is proportional to the imaginary part of the self-energy and describes the lifetime broadening $\hbar/\tau$ of the excited photohole [17,18]. In general, the linewidth Γ of surface states on clean metal surfaces is determined by electron-electron $\Gamma_{e\text{-}e}$ and electron-phonon $\Gamma_{e\text{-}p}$ scattering [27,28]. In addition, defect scattering can lead to a usually temperature-independent contribution to the photoemission linewidth Γ_d [29]. In case of ferromagnetic surfaces electron-magnon scattering can additionally lead to a spin-dependent linewidth $\Gamma_{e\text{-}m}$ [30]. The total linewidth is the sum of these contributions, which can in part be separated by their different temperature dependence.

A. Linewidth of the Gd surface state

First, we will concentrate on the linewidth of the Gd surface state [Fig. 3(a)], which shows a pronounced spin dependence. This must be related to spin-dependent scattering processes filling the excited photohole.

Let us start with a *Gedanken* experiment, the perfect example of the ferromagnetic ground state, i.e., for temperature $T \to 0$. As in the sf model [31] we consider a single valence electron interacting with the fully aligned $4f$ spin systems. Parallel and antiparallel alignment of the valence-electron spin with respect to the $4f$ spins leads to exchange splitting of majority and minority spin bands. A spin-flip excitation of a majority spin valence electron is not possible since angular momentum conservation would require absorption of a magnon [30], which is not excited in the ground state. As a consequence the majority spin band is only rigidly shifted. Spin-flip scattering is only possible for minority valence electrons exciting spin waves in the $4f$ system. Depending on the ratio of exchange interaction J and bandwidth W this process leads to broadening of the valence band and shifts of the spectral weight [31]. Considering a fully occupied band with a single photohole, as in our experiment, we have to exchange the role of majority and minority spin state. Thus for $T \to 0$, we would expect contributions of spin-flip scattering only to the linewidth of the majority spin component due to magnon emission. As evident from Fig. 3(a) for Gd we

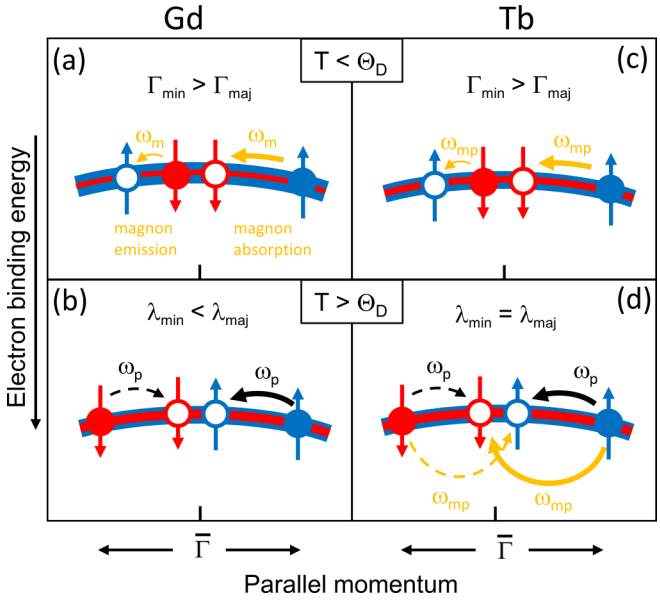

FIG. 4. Sketch of *intra*-band scattering processes filling the photohole (open circle) in the occupied surface state band of Gd (left column) and Tb (right column). Blue and red colors denote the spin majority and spin minority components, respectively. The degree of spin mixing of the surface-state band is indicated by the line thickness. **Gd** (a) In the temperature range $T < \Theta_D$ between 90 and 160 K electron-magnon scattering (ω_m) dominates. This leads in combination with the spin-dependent density of states to larger lifetime broadening in the spin minority channel $\Gamma_{min} > \Gamma_{maj}$. (b) For $T > \Theta_D$ spin conserving electron-phonon scattering dominates and leads to a spin-dependent mass-enhancement parameter $\lambda^{Gd}_{min} < \lambda^{Gd}_{maj}$. **Tb** (c) For $T < \Theta_D$ electron-(magnon-polaron) scattering (ω_{mp}) dominates and $\Gamma_{min} > \Gamma_{maj}$. (d) For $T > \Theta_D$ phonon scattering and magnon-polaron formation double the phase space for electron scattering and $\lambda^{Tb}_{min} = \lambda^{Tb}_{maj} = (\lambda^{Gd}_{min} + \lambda^{Gd}_{maj})$.

observe the opposite behavior in the temperature range between 90 and 160 K. The linewidth for the majority spin component $\Gamma^{Gd}_{maj} \sim 130$ meV is smaller than the linewidth of the minority spin component $\Gamma^{Gd}_{min} \sim 150$ meV. For Gd the maximum magnon energy is around 25 meV [12]. Thus above 90 K (7.5 meV) a sizable fraction of spin waves is already excited and both magnon emission and absorption will lead to filling of the excited photohole. Considering *intra*-band scattering, i.e., electron and hole stay within the occupied surface-state band, these processes require only small momentum transfer and magnon energies. We thus argue that around 90 K the spin-dependence results from the finite spin polarization of the surface state. For a spin polarization P of about 55% we have on average 3.4 times more majority spin electrons in the spin-mixed surface band than minority spin electrons [*cf.* Figs. 1(a) and 2(b)]. As illustrated in Fig. 4(a) filling of a minority spin photohole at $\bar{\Gamma}$ by magnon absorption $\omega_m(\pm q)$ leads to a majority photohole at $E_0(\bar{\Gamma} \mp q) + \hbar\omega_m$ (the binding energy of the electron is reduced by magnon absorption). The opposite process of filling of a majority spin photohole with a minority spin electron by magnon emission is less efficient, due to the finite spin polarization. Besides *intra*-band scattering, *inter*-band scattering between electronic bulk and surface states will contribute to filling of the photohole. In general the same arguments as for *intra*-band scattering will apply, since the bulk density of states is spin polarized (see Ref. [32], Fig. 3 and Ref. [14], Fig. 8 of the SM). However, the effect may be less pronounced, since it requires magnons with larger momentum and thus energy transfer. For these magnons emission $\propto n + 1$ will be stronger than absorption $\propto n$ at around 90 K, which counteracts the effect of the spin polarization [$n = (\exp(\hbar\omega/k_BT) - 1)^{-1}$ is the number of excited magnons].

The linewidth of the Gd surface state was previously studied experimentally and theoretically by Fedorov and Allen [17,18]. They concluded that at low temperature magnon emission leads to a filling of the minority spin photohole and calculated a linewidth broadening of $\Gamma_{min} \sim 95$ meV as opposed to $\Gamma_{maj} \sim 14$ meV for a spin polarization of 0.87 reached at 20 K sample temperature. The Lorentzian broadenings in the experiment were 116 meV and 86 meV, respectively. While we observe the same trend and similar difference between Γ_{min} and Γ_{maj}, we argue that filling occurs by magnon absorption. The latter process is compatible with angular momentum and energy conversion as depicted in Fig. 4(a).

With increasing temperature $T \geqslant 160$ K the linewidth Γ starts to increase linearly with T [Fig. 3(a)]. For Gd the spin dependence is now reversed; the slope for the majority spin component is larger than for the minority spin component. Using again the above phase space argument we attribute this spin dependence to electron-phonon scattering. The spin-flip probability for Gd upon scattering of valence electrons with phonons is estimated to be $\alpha = 0.08$ [6]. Thus, when scattering with a phonon the electron spin remains predominantly unchanged and, as sketched in Fig. 4(b), the photohole in the majority (minority) spin channel is filled by majority (minority) spin electrons.

The Debye temperature Θ_D of Gd and Tb are reported to be about 163 and 176 K [33,34]. At the surface Θ^s_D is further reduced by a factor of 0.6 ± 0.1 with respect to the bulk value [35]. For high temperatures $T > \Theta_D \gg \Theta^s_D$ the Debye model predicts a linear dependence of the scattering rate $\Gamma_{e\text{-}p} = 2\pi\lambda k_b T$, since the number of phonons increases linearly with temperature $n \to k_BT/\hbar\omega$, for $\hbar\omega \sim k_B\Theta_D \ll k_BT$. Within experimental error we observe a constant slope in our experimental data for $T \geqslant 160$ K [Fig. 3(a)]. Fitting the data for the Gd surface state within the temperature range of 150 to 270 K (see SM) [26], we obtain the spin-dependent mass-enhancement parameters of $\lambda_{maj} = 1.02 \pm 0.2$ and $\lambda_{min} = 0.88 \pm 0.2$. This compares well with the reported values of a previous photoemission experiment for the majority spin component $\lambda_{maj} = 1.0 \pm 0.2$ [18] and spin-averaged values of scanning tunneling spectroscopy (STS) $\lambda = 1.0 \pm 0.2$ [36]. As obvious from Fig. 2 the spin-dependent density of states (spin polarization) available for scattering varies with temperature due to spin mixing. Here electron-phonon and electron-magnon scattering will show opposite trends. This may partially cancel the temperature dependence expected for λ. We note that electron-magnon and electron-phonon scattering increase with the number of excited magnons and phonons n. Since both have comparable energies one would at first glance expect similar temperature dependences. However, the interaction is completely different, determined

for magnons by exchange coupling J and for phonons by deformation-potential scattering. While the former is temperature independent, the latter will increase with the amplitude of lattice vibrations and thus with temperature. This explains qualitatively why the lifetime broadening of the Gd surface state is determined at low temperature by electron-magnon and at high temperature by electron-phonon scattering.

So far we have only considered *intra*-band scattering, i.e., relaxation processes within the surface-state band, but neglected *inter*-band scattering involving bulk states. Relaxation of the photohole by inelastic electron-electron scattering requires excitation of electron hole pairs across the Fermi level. Therefore $\Gamma_{\text{e-e}}$ is approximately proportional to the available phase space $\propto (E - E_F)^2$. STS measurements show a total linewidth of only 22 meV at $T \sim 10$ K [37]. With increasing temperature the occupied component of the surface state shifts towards E_F [*cf.* Fig. 2(a)], decreasing the phase space for electron-electron scattering. Thus STS sets the maximum contribution of $\Gamma_{\text{e-e}}$ to 22 meV. Since the occupied surface state lies within the band gap of surface-projected majority spin bulk states, defect and electron-phonon scattering involving bulk states will lead to larger broadening of the majority spin component of the occupied surface state than of its minority spin counterpart. Thus electron-phonon *inter*-band scattering can contribute to the observed spin and temperature-dependence of the mass-enhancement factor $\lambda_{\text{maj}} > \lambda_{\text{min}}$ of the Gd surface state.

B. Linewidth of the Tb surface state

In the second step, we turn to the linewidth of the Tb surface state [Fig. 3(b)]. Since Tb and Gd films have comparable hexagonal-closed packed crystal structure and very similar valence band structures, we would expect electron-magnon and electron-phonon scattering to contribute similarly to the linewidth of the Tb and Gd surface states.

Owing to the lower maximal magnon energy of 15 meV we observe a somewhat lower spin polarization of the Tb surface state of 40% at around 100 K. Still this corresponds to a 2.3 times higher majority spin contribution [*cf.* Figs. 1(a) and 2(b)]. In line with the lower spin polarization, the Tb surface state shows the same trend $\Gamma_{\text{min}} > \Gamma_{\text{maj}}$ but less pronounced as compared to Gd. However, as evident from Fig. 3(b) the linewidth of the Tb surface state above $T = 150$ K does not show a significant spin dependence. This suggests that Γ is not dominated by pure electron-magnon and electron-phonon scattering in the high temperature regime.

The only key difference between Tb and Gd is the strong $4f$ spin-orbit coupling (SOC) in Tb ($4f^8$, $L = 3$) which is negligible in Gd ($4f^7$, $L = 0$). The different SOC can be understood when considering the orbital distribution. As illustrated in Fig. 5 for Gd it is spherical symmetric (blue sphere), while for Tb it can be represented by the additional electron in the $m_\ell = 3$ sublevel (blue torus). Therefore, vibrations of the lattice ions (gray balls) will affect the charge distribution of Tb but not of Gd. As a consequence, phonons couple to the orbital momentum and thus the $4f$ spin (red arrow) of Tb but not of Gd. Likewise magnons will only couple to the Tb lattice. The strong SOC in Tb is also reflected in a large magnetocrystalline anisotropy (16.5 meV for Tb vs 0.03 meV

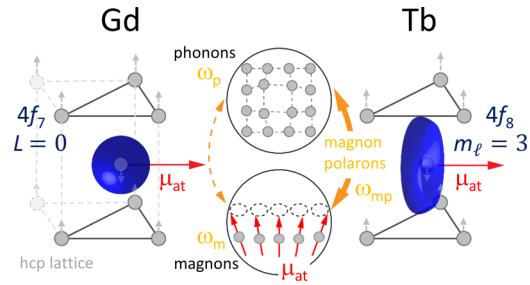

FIG. 5. Illustration of weak and strong phonon-magnon hybridization in Gd and Tb, respectively. While the Gd $4f^7$ charge distribution has a spherical shape ($L = 0$) that of the Tb $4f^8$ state ($L = 3$) can be represented by the $m_\ell = 3$ component. Rocking of the lattice ions couples only to the nonspherical charge distribution of Tb [8].

for Gd) [38,39] and is essential to couple motion of the lattice ions via the orbital angular momentum to $4f$ spin excitations [8,40]. Moreover, for Tb the magnitude of the planar anisotropy constant found in static measurements is much smaller than the value necessary for agreement with spin-wave experiments, indicating a significant contribution of magnetoelastic effects to the total hexagonal planar anisotropy constant [41]. Neutron diffraction shows strong splitting of transversal optical phonon (TO) and acoustic magnon (AM) branches near the BZ boundary [42,43] and weaker splitting of magnetoacoustical and transversal acoustical (TA) phonon branches [40]. The latter AM-TA coupling can be explained by local strain in an ff model [40,44]. It leads to an avoided crossing of magnon and phonon dispersions in an energy range of about 2–4 meV associated with small momentum transfer of 0.1–0.3 Å^{-1}. These magnon polarons are already sufficiently excited at 100 K. The avoided crossing between the TO and AM branches is more involved since their coupling is symmetry forbidden [40]. Based on a proposal by Liu [45], Jensen and Houmann showed that this coupling can be induced by spin mixing in the valence states, which is proportional to spin-orbit coupling of the valence states [40]. This involves the already introduced sf model, which couples the valence electrons via *intra*-atomic exchange to the magnon polarons [see Fig. 4(c)]. As a consequence, whenever a phonon is emitted it can effectively couple to a magnon excitation, becoming a magnon polaron. The linewidth data in Fig. 3(b) show this characteristic of the magnon-phonon hybridization in Tb. At temperatures $T > T_{\text{D}}$ where $\Gamma \propto T$, the mass-enhancement parameters of Tb is $\lambda^{\text{maj}}_{\text{e-ph}} = \lambda^{\text{min}}_{\text{e-ph}} = 1.7 \pm 0.1$, i.e., identical within error bars. Thus for Tb the mass enhancement parameter is twice as large as the average value of Gd $\lambda_{\text{e-ph}}(\text{Tb}) = \lambda^{\text{maj}}_{\text{e-ph}}(\text{Gd}) + \lambda^{\text{min}}_{\text{e-ph}}(\text{Gd})$. The phase space is nearly doubled for Tb as compared to Gd which necessarily includes magnon contributions. This is a direct consequence of magnon-polaron formation in Tb. As sketched in Fig. 4(d) contributions of electron-phonon and electron-(magnon-polaron) scattering lead to comparable linewidth of majority and minority spin photoholes. In fact, significant damping of coherent phonons in Tb by coupling to magnons has already been demonstrated with time-resolved second harmonic spectroscopy [13].

IV. SUMMARY

In conclusion, comparing Gd and Tb we demonstrate the role of magnon-polaron formation in the lifetime broadening of the Tb surface state. For Gd we observe a spin-dependent lifetime broadening, which reflects the degree of band mirroring. At 100 K, the linewidth of the spin-minority component is larger than its spin-majority counterpart, which is attributed to electron-magnon scattering. Above the Debye temperature we observe a linear increase of the linewidth due to spin-conserving electron-phonon scattering. Accordingly the mass enhancement parameter is larger for the spin majority than for the spin minority component.

Meanwhile for the Tb surface state the linewidth is comparable in both spin channels with no spin dependence above 150 K. The fitted electron-phonon mass-enhancement parameter in Tb is twice as large as the average value in Gd, suggesting that both spin-flip and spin-conserving scattering processes contribute to the linewidth. Considering the large magnetoelastic coupling in Tb that can induce hybrid magnon-phonon modes, we suggest that magnon-polaron formation adds significantly to the linewidth broadening of the Tb surface state.

In the present study we show that magnon-polaron generation in Tb occurs by scattering of optically excited valence electrons (holes). Because the $5d_{z^2}$ surface state of Gd and Tb is derived from bulk states, we can reasonably assume that surface and bulk valence states will show in each case similar couplings. This allows us to explain the efficient ultrafast demagnetization of the $4f$ spin system in Tb [14] and the in contrast disparate dynamics of $5d$ and $4f$ spin systems in Gd [21]. While in Tb coupling of the photoexcited valence electrons and holes to the lattice is accompanied by effective generation of magnons, the latter process is missing in Gd.

Our findings contribute to the fundamental understanding of ultrafast magnetization dynamics revealing its signature in the electronic structure. Strong spin-orbit coupling in $4f$ systems couples excited valence electrons and holes effectively to the $4f$ spin system via lattice excitations.

The photoemission data used for the presented analysis are publicly available [46].

ACKNOWLEDGMENTS

This project was supported by the Deutsche Forschungsgemeinschaft through Collaborative Research Center TRR 227 on Ultrafast SpinDynamics, project A01. H.X. is indebted to the China Scholarship Council for financial support.

[1] H. Hayashi and K. Ando, Spin Pumping Driven by Magnon Polarons, Phys. Rev. Lett. **121**, 237202 (2018).

[2] J. Holanda, D. S. Maior, A. Azevedo, and S. M. Rezende, Detecting the phonon spin in magnon-phonon conversion experiments, Nat. Phys. **14**, 500 (2018).

[3] T. Kikkawa, K. Shen, B. Flebus, R. A. Duine, K.-ichi Uchida, Z. Qiu, G. E. W. Bauer, and E. Saitoh, Magnon Polarons in the Spin Seebeck Effect, Phys. Rev. Lett. **117**, 207203 (2016).

[4] R. Ramos, T. Hioki, Y. Hashimoto, T. Kikkawa, P. Frey, A. J. E. Kreil, V. I. Vasyuchka, A. A. Serga, B. Hillebrands, and E. Saitoh, Room temperature and low-field resonant enhancement of spin Seebeck effect in partially compensated magnets, Nat. Commun. **10**, 5162 (2019).

[5] M. Battiato, K. Carva, and P. M. Oppeneer, Superdiffusive Spin Transport as a Mechanism of Ultrafast Demagnetization, Phys. Rev. Lett. **105**, 027203 (2010).

[6] B. Koopmans, G. Malinowski, F. Dalla Longa, D. Steiauf, M. Fähnle, T. Roth, M. Cinchetti, and M. Aeschlimann, Explaining the paradoxical diversity of ultrafast laser-induced demagnetization. Nat. Mater. **9**, 259 (2010).

[7] A. Vaterlaus, T. Beutler, and F. Meier, Spin-Lattice Relaxation Time of Ferromagnetic Gadolinium Determined with Time-Resolved Spin-Polarized Photoemission, Phys. Rev. Lett. **67**, 3314 (1991).

[8] M. Wietstruk, A. Melnikov, C. Stamm, T. Kachel, N. Pontius, M. Sultan, C. Gahl, M. Weinelt, H. A. Dürr, and U. Bovensiepen, Hot-Electron-Driven Enhancement of Spin-Lattice Coupling in Gd and Tb 4f Ferromagnets Observed by Femtosecond X-Ray Magnetic Circular Dichroism, Phys. Rev. Lett. **106**, 127401 (2011).

[9] A. Eschenlohr, M. Sultan, A. Melnikov, N. Bergeard, J. Wieczorek, T. Kachel, C. Stamm, and U. Bovensiepen, Role of spin-lattice coupling in the ultrafast demagnetization of $Gd_{1-x}Tb_x$ alloys, Phys. Rev. B **89**, 214423 (2014).

[10] J.-W. Kim, M. Vomir, and J.-Y. Bigot, Ultrafast Magnetoacoustics in Nickel Films, Phys. Rev. Lett. **109**, 166601 (2012).

[11] S. Zeuschner, T. Parpiiev, T. Pezeril, A. Hillion, K. Dumesnil, A. Anane, J.-E. Pudell, L. Willig, M. Rössle, M. Herzog, A. v. Reppert, and M. Bargheer, Tracking picosecond strain pulses in heterostructures that exhibit giant magnetostriction, Struc. Dyn. **6**, 024302 (2019).

[12] J. Jensen and A. R. Mackintosh, *Rare Earth Magnetism, Structures and Excitations* (Clarendon Press, Oxford, 1991).

[13] A. Melnikov, A. Povolotskiy, and U. Bovensiepen, Magnon-Enhanced Phonon Damping at Gd(0001) and Tb(0001) Surfaces Using Femtosecond Time-Resolved Optical Second-Harmonic Generation, Phys. Rev. Lett. **100**, 247401 (2008).

[14] B. Frietsch, A. Donges, R. Carley, M. Teichmann, J. Bowlan, K. Döbrich, K. Carva, D. Legut, P. M. Oppeneer, U. Nowak, and M. Weinelt, The role of ultrafast magnon generation in the magnetization dynamics of rare-earth metals, Sci. Adv. **6**, eabb1601 (2020).

[15] R. Gort, K. Bühlmann, S. Däster, G. Salvatella, N. Hartmann, Y. Zemp, S. Holenstein, C. Stieger, A. Fognini, T. U. Michlmayr, T. Bähler, A. Vaterlaus, and Y. Acremann, Early Stages of Ultrafast Spin Dynamics in a 3*d* Ferromagnet, Phys. Rev. Lett. **121**, 087206 (2018).

[16] R. Gort, K. Bühlmann, G. Saerens, S. Däster, A. Vaterlaus, and Y. Acremann, Ultrafast magnetism: The magneto-optical Kerr effect and conduction electrons, Appl. Phys. Lett. **116**, 112404 (2020).

[17] P. B. Allen, Electron spin-flip relaxation by one magnon processes: Application to the gadolinium surface band, Phys. Rev. B **63**, 214410 (2001).

[18] A. V. Fedorov, T. Valla, F. Liu, P. D. Johnson, M. Weinert, and P. B. Allen, Spin-resolved photoemission study of photohole lifetimes in ferromagnetic gadolinium, Phys. Rev. B **65**, 212409 (2002).

[19] A. Winkelmann, D. Hartung, H. Engelhard, C.-T. Chiang, and J. Kirschner, High efficiency electron spin polarization analyzer based on exchange scattering at Fe/W(001), Rev. Sci. Instrum. **79**, 083303 (2008).

[20] Kh. Zakeri, T. R. F. Peixoto, Y. Zhanga, J. Prokopa, and J. Kirschner, On the preparation of clean tungsten single crystals, Surf. Sci. **604**, L1 (2010).

[21] B. Frietsch, J. Bowlan, R. Carley, M. Teichmann, S. Wienholdt, D. Hinzke, U. Nowak, K. Carva, P. M. Oppeneer, and M. Weinelt, Disparate ultrafast dynamics of itinerant and localized magnetic moments in gadolinium metal, Nat. Commun. **6**, 8262 (2015).

[22] B. Andres, M. Christ, C. Gahl, M. Wietstruk, M. Weinelt, and J. Kirschner, Separating Exchange Splitting from Spin Mixing in Gadolinium by Femtosecond Laser Excitation, Phys. Rev. Lett. **115**, 207404 (2015).

[23] M. Bode, M. Getzlaff, A. Kubetzka, R. Pascal, O. Pietzsch, and R. Wiesendanger, Temperature-Dependent Exchange Splitting of A Surface State on A Local-Moment Magnet: Tb(0001), Phys. Rev. Lett. **83**, 3017 (1999).

[24] K. Maiti, M. C. Malagoli, A. Dallmeyer, and C. Carbone, Finite Temperature Magnetism in Gd: Evidence Against a Stoner Behavior, Phys. Rev. Lett. **88**, 167205 (2002).

[25] M. Teichmann, B. Frietsch, K. Döbrich, R. Carley, and M. Weinelt, Transient band structures in the ultrafast demagnetization of ferromagnetic gadolinium and terbium, Phys. Rev. B **91**, 014425 (2015).

[26] See Supplemental Material at http://link.aps.org/supplemental/10.1103/PhysRevB.104.024434 for information on experimental resolution, peak fitting, and evaluation of the spin-dependent mass-enhancement parameter λ.

[27] J. Kliewer, R. Berndt, E. V. Chulkov, V. M. Silkin, P. M. Echenique, and S. Crampin, Dimensionality effects in the lifetime of surface states, Science **288**, 1399 (2000).

[28] P. M. Echenique, R. Berndt, E. V. Chulkov, Th. Fauster, A. Goldmann, and U. Höfer, Decay of electronic excitations at metal surfaces, Surf. Sci. Rep. **52**, 219 (2004).

[29] F. Reinert, G. Nicolay, S. Schmidt, D. Ehm, and S. Hüfner, Direct measurements of the L-gap surface states on the (111) face of noble metals by photoelectron spectroscopy, Phys. Rev. B **63**, 115415 (2001).

[30] A. B. Schmidt, M. Pickel, M. Donath, P. Buczek, A. Ernst, V. P. Zhukov, P. M. Echenique, L. M. Sandratskii, E. V. Chulkov, and M. Weinelt, Ultrafast Magnon Generation in an Fe Film on Cu(100), Phys. Rev. Lett. **105**, 197401 (2010).

[31] S. Rex, V. Eyert, and W. Nolting, Temperature-dependent quasiparticle bandstructure of ferromagnetic gadolinium, J. Magn. Magn. Mater. **192**, 529 (1999).

[32] Ph. Kurz, G. Bihlmayer, and S. Blügel, Magnetism and electronic structure of hcp Gd and the Gd(0001) surface, J. Phys.: Condens. Matter **14**, 6353 (2002).

[33] T. W. E. Tsang, K. A. Gschneidner, F. A. Schmidt, and D. K. Thome, Low-temperature heat capacity of electrotransport-purified scandium, yttrium, gadolinium, and lutetium, Phys. Rev. B **31**, 235 (1985).

[34] H. L. Skriver and I. Mertig, Electron-phonon coupling in the rare-earth metals, Phys. Rev. B **41**, 6553 (1990).

[35] E. Weschke, A. Höhr, S. Vandré, C. Schüßler-Langeheine, F. Bødker, and G. Kaindl, Thermal effects on photoemission spectra of lanthanide metals, J. Electron Spectrosc. Relat. Phenom. **76**, 571 (1995).

[36] A. Rehbein, D. Wegner, G. Kaindl, and A. Bauer, Temperature dependence of lifetimes of Gd(0001) surface states, Phys. Rev. B **67**, 033403 (2003).

[37] D. Wegner, A. Bauer, and G. Kaindl, Magnon-broadening of exchange-split surface states on lanthanide metals, Phys. Rev. B **73**, 165415 (2006).

[38] J. Rhyne and A. E. Clark, Magnetic anisotropy of terbium and dysprosium, J. Appl. Phys. **38**, 1379 (1967).

[39] S. Abdelouahed and M. Alouani, Magnetic anisotropy in Gd, GdN, and $GdFe_2$ tuned by the energy of gadolinium 4f states, Phys. Rev. B **79**, 054406 (2009).

[40] J. Jensen and J. G. Houmann, Spin waves in terbium. ii. magnon-phonon interaction, Phys. Rev. B **12**, 320 (1975).

[41] B. R. Cooper, Spin waves and magnetic resonance in rare-earth metals: Thermal, applied-field, and magnetoelastic effects, Phys. Rev. **169**, 281 (1968).

[42] H. B. Møller, J. C. G. Houmann, and A. R. Mackintosh, Magnetic Interactions in Rare-Earth Metals from Inelastic Neutron Scattering, Phys. Rev. Lett. **19**, 312 (1967).

[43] M. Nielsen, H. B. Møller, and A. R. Mackintosh, Magnon interactions in terbium, J. Appl. Phys. **41**, 1174 (1970).

[44] D. T. Vigren and S. H. Liu, Static and dynamic effects of the magnetoelastic interaction in terbium and dysprosium metals, Phys. Rev. B **5**, 2719 (1972).

[45] S. H. Liu, New Magnetoelastic Interaction, Phys. Rev. Lett. **29**, 793 (1972).

[46] B. Liu, H. Xiao, G. Siemann, J. Weber, B. Andres, W. Bronsch, P. M. Oppeneer, and M. Weinelt, Dataset for "Signature of magnon polarons in electron relaxation on terbium revealed by comparison with gadolinium", https://zenodo.org/record/5116307#.YPhAPOgzZaQ, Zenodo, 2021.